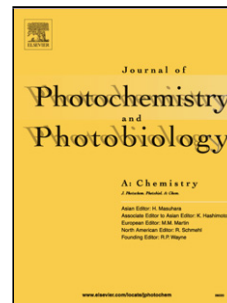


## Accepted Manuscript

Title: The simplest molecular chemosensor for detecting higher pHs,  $\text{Cu}^{2+}$  and  $\text{S}^{2-}$  in aqueous environment and executing various logic gates

Authors: Awad I. Said, Nikolai I. Georgiev, Vladimir B. Bojinov



PII: S1010-6030(18)31404-7  
DOI: <https://doi.org/10.1016/j.jphotochem.2018.11.029>  
Reference: JPC 11601

To appear in: *Journal of Photochemistry and Photobiology A: Chemistry*

Received date: 27 September 2018  
Revised date: 7 November 2018  
Accepted date: 19 November 2018

Please cite this article as: Said AI, Georgiev NI, Bojinov VB, The simplest molecular chemosensor for detecting higher pHs,  $\text{Cu}^{2+}$  and  $\text{S}^{2-}$  in aqueous environment and executing various logic gates, *Journal of Photochemistry and Photobiology, A: Chemistry* (2018), <https://doi.org/10.1016/j.jphotochem.2018.11.029>

This is a PDF file of an unedited manuscript that has been accepted for publication. As a service to our customers we are providing this early version of the manuscript. The manuscript will undergo copyediting, typesetting, and review of the resulting proof before it is published in its final form. Please note that during the production process errors may be discovered which could affect the content, and all legal disclaimers that apply to the journal pertain.

# The simplest molecular chemosensor for detecting higher pHs, $\text{Cu}^{2+}$ and $\text{S}^{2-}$ in aqueous environment and executing various logic gates

Awad I. Said <sup>a,b</sup>, Nikolai I. Georgiev <sup>a</sup>, Vladimir B. Bojinov <sup>a\*</sup>

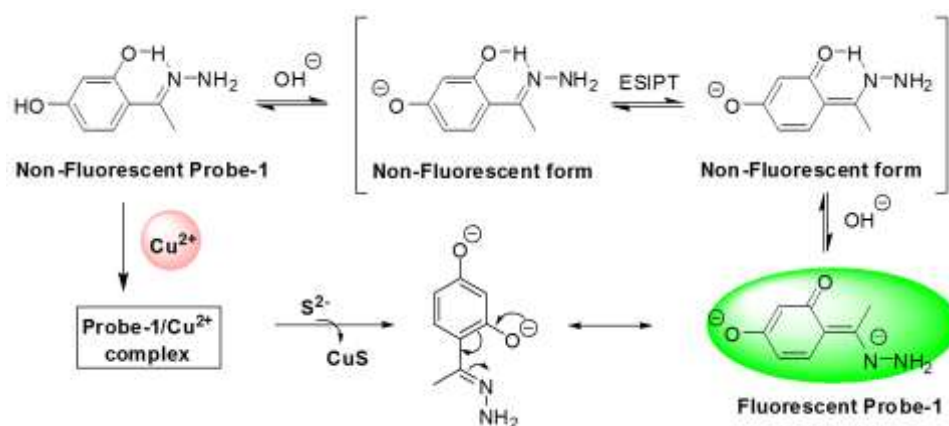
<sup>a</sup> *Department of Organic Synthesis, University of Chemical Technology and Metallurgy, 8 Kliment Ohridsky Str., 1756 Sofia, Bulgaria*

<sup>b</sup> *Department of Chemistry, Faculty of Science. Assiut University, Assiut, Egypt*

---

\* Corresponding author. Tel.: (+ 359 2) 8163206  
E-mail address: [vlbojin@uctm.edu](mailto:vlbojin@uctm.edu) (V. B. Bojinov)

## Graphical abstract



## Highlights

- A highly water-soluble in alkaline window hydrazone derivative is synthesized.
- Hydrazone derivative acts as a molecular fluorescent pH probe.
- Probe manifests selective fluorescence response to  $\text{Cu}^{2+}$  in alkaline aqueous medium.
- Probe/ $\text{Cu}^{2+}$  complex serves as a highly sensitive molecular sensor for  $\text{S}^{2-}$  anions.
- A series of logic gates of the probe are achieved.

## A B S T R A C T

The sensory properties of the simplest Probe-1 are reported. Probe-1 exhibits colorimetric and fluorimetric responses towards higher pHs. Also, a borate aqueous solution of Probe-1 (pH = 10) could to detect the presence of  $\text{Cu}^{2+}$  in aqueous solution with high selectivity and sensitivity (3  $\mu\text{M}$ ). The Probe-1/ $\text{Cu}^{2+}$  complex responses selectively towards the presence of  $\text{S}^{2-}$ ,  $\text{H}_2\text{PO}_4^-$  and  $\text{P}_2\text{O}_7^{4-}$  through a de-metallization mechanism, resulting in a fluorescence enhancement of 143%, 97% and 134%, respectively. On the other hand, the Probe-1 absorbance increases significantly only by  $\text{S}^{2-}$  (131%). Furthermore, Probe-1 executes many logic gates such as *XOR*, *AND*, *INHIBIT*, *IMPLICATION*, *TRANSFER* and *NOT TRANSFER*.

**Keywords:** (*E*)-4-(1-hydrazoneethyl)benzene-1,3-diol; Fluorescence probe; Detection of  $\text{Cu}^{2+}$ ,  $\text{S}^{2-}$  and  $\text{H}_2\text{PO}_4^-$ ; De-metallization; *AND*, *XOR*, *INHIBIT*, *IMPLICATION*, *TRANSFER* and *NOT TRANSFER* logic gates.

---

## 1. Introduction

pH plays an important role in most biological and industrial processes [1-8]. Although electrochemical pH sensors are well known as a reliable tool for solving different tasks, some disadvantages of pH electrodes, including the need for continuous calibration, a frequent electrical interference and possibility of corrosion in alkaline media, greatly limit their effectiveness [9]. Therefore, the considerable efforts of the researchers in recent years have been directed towards the creation of optical sensors for detecting pH changes in the environment [10-12], operating via different sensing mechanisms [13-18]. Among these, molecular fluorescent pH sensors have gained a significant attention because of their high sensitivity [19-22].

$\text{Cu}^{2+}$ , the third by quantity transition metal ion in the human body, has an important role in numerous of physiological processes [23-25]. Overloading of copper in neuronal cytoplasm is associated with Wilson and Alzheimer diseases [26,27]. That is why a number of researchers have made serious efforts to develop molecular probes for detecting Cu(II) [28-43]. Although a  $\text{Cu}^{2+}$  bound fluorophore usually causes a fluorescence quenching due to the paramagnetic nature of  $\text{Cu}^{2+}$ , the non-fluorescent  $\text{Cu}^{2+}$ -fluorophore complex can provide an indirect route for anion (as sulfide) recognition through  $\text{Cu}^{2+}$  demetallization approach [44]. Sulfides are widespread in the environment and find significant use in the production of sulfur, sulfuric acid, dyes and cosmetics [45]. Nevertheless, higher doses of sulfide lead to unpleasant physiological problems such as mucosal irritation, loss of consciousness and respiratory paralysis [46].

A series of methods for the recognition of Cu(II) have been developed [47-49]. All of them, however, unlike fluorescence probes, use time-consuming procedures and expensive toolkit [50,51]. In the recent years many excellent chemosensors and chemodosimeters for Cu(II) have been described. However, some of them have various shortcomings including complicated synthetic procedures, high detection limit, use of organic solvents and interference from other transition metals ions, which often coexist and have similar reactivity toward molecular sensors [52-54]. Chemosensors containing 2-hydroxyl hydrazone are well known for their ability to chelate and detect transition metal cations, especially  $\text{Cu}^{2+}$  [55,56].

Incorporation of the molecule scale into information technology in performing the required logic gates and operations is a challenge since the last decades. Many scientists have

focused on the design of smart functional molecular systems capable of working as Boolean logic gates as well as could to execute several high order functions like comparator [57-62], half-adder/subtractor [63-65], memory device [66,67], key-pad lock [68,69], etc. These can mimic modern semiconductor based devices to a dimension as small as in the nanoscale order.

In a previous work, we examined some photophysical characteristics of hydrazone of 2,4-dihydroxyacetophenone depending on the pH of the medium [57]. In this work, we synthesized 2,4-dihydroxyl acetophenone hydrazone (Probe-1) by improved synthetic procedure and investigated its unexpectedly interesting properties and the benefit to operate as a simple fluorescent probe for pH and  $\text{Cu}^{2+}$ . Probe-1 simultaneously performs both receptor and reporter functions and is capable of selectively recognizing  $\text{Cu}^{2+}$  in the presence of other representative transition metal ions. Also, we investigated the aptitude of the  $\text{Cu}^{2+}$ /Probe-1 complex for the detection of sulfide and the selectivity of this detection as well as the ability of the compound to execute different logical operations.

## 2. Experimental

### 2.1. Materials

Commercially available 2,4-dihydroxyacetophenone (Aldrich) and hydrazine monohydrate (Aldrich) were used as delivered. All solvents (Fisher Chemical, Aldrich) were pure or of spectroscopy grade. All used salts as sources for metal ions  $\text{Zn}(\text{NO}_3)_2$ ,  $\text{Cu}(\text{NO}_3)_2$ ,  $\text{Ni}(\text{NO}_3)_2$ ,  $\text{Co}(\text{NO}_3)_2$ ,  $\text{Pb}(\text{NO}_3)_2$ ,  $\text{Fe}(\text{NO}_3)_3$ ,  $\text{Hg}(\text{NO}_3)_2$ ,  $\text{Cd}(\text{NO}_3)_2$ ,  $\text{Cr}(\text{NO}_3)_3$  and  $\text{AgNO}_3$  or anions  $\text{NaF}$ ,  $\text{Na}_2\text{SO}_4$ ,  $\text{NaHSO}_4$ ,  $\text{NaNO}_2$ ,  $\text{Na}_2\text{S}_2\text{O}_5$ ,  $\text{CH}_3\text{COONa}$ ,  $\text{Na}_2\text{CO}_3$ ,  $\text{NaCN}$ ,  $\text{Na}_2\text{S}$ ,  $\text{KBr}$ ,  $\text{NaH}_2\text{PO}_4$  and  $\text{Na}_4\text{P}_2\text{O}_7$  were of pure for analysis grade.

### 2.2. Methods

FT-IR spectrum was taken on a Varian Scimitar 1000 spectrometer. The  $^1\text{H}$  NMR spectrum was registered on a Bruker DRX-250 spectrometer. Kofler microscope was used for the determination of melting point. Absorption and fluorescence spectra were recorded on a Hewlett Packard 8452A and Scinco FS-2 spectrophotometers, respectively. The excitation source for the fluorescence measurements was a 150 W Xenon lamp and the excitation/emission slits width was 5 nm.

### 2.3. Synthesis of (*E*)-4-(1-hydrazonoethyl)benzene-1,3-diol (*Probe-1*)

A mixture of 2,4-dihydroxyacetophenone (15.2 g, 100 mmol) and 46 mL of hydrazine monohydrate was stirred for 4 h at room temperature in 50 mL of DMF. Then the reaction mixture was diluted with 100 mL of water. The precipitate was filtered off and washed with fresh water to give 16.1 g (97%) of desired compound (*Probe-1*). M.p 196-198°C;  $R_f = 0.32$  in ethyl acetate/petroleum ether = (2:1).

FT-IR (KBr)  $\text{cm}^{-1}$ : 3292 ( $\nu_{\text{OH}}$ ,  $\nu_{\text{NH}}$ ); 2924 ( $\nu_{\text{CH}}$ ); 1599 ( $\nu_{\text{C=N}}$ ).  $^1\text{H NMR}$  ( $\text{CHCl}_3$ -*d*, 250.13 MHz)  $\delta$  ppm: 12.96 (s, 1H, Ph-OH); 11.08 (s, 1H, Ph-OH); 7.58 (d, 1H,  $J = 8.8$  Hz, Ph-H5); 6.39 (dd, 1H,  $J = 8.8$  Hz,  $J = 2.4$  Hz, Ph-H6); 6.22 (d, 1H,  $J = 2.4$  Hz, Ph-H2); 3.29 (s, 2H,  $\text{NH}_2$ ); 2.54 (s, 3H,  $\text{CH}_3$ ). Elemental analysis: Calculated for  $\text{C}_8\text{H}_{10}\text{N}_2\text{O}_2$  (MW 166.18) C 57.82, H 6.07, N 16.86 %; Found C 57.48, H 6.15, N 16.58 %.

## 3. Results and discussion

### 3.1 Designing and synthesis of *Probe-1*

*Probe-1* was prepared simply according to an improved previously described synthetic procedure [57] by stirring 2,4-dihydroxyl acetophenone with excess of hydrazine hydrate in DMF solution at room temperature instead of under reflux for the same duration of 4 hours (Scheme 1).

**Insert here Scheme 1**

As we demonstrated before, (*E*)-4-(1-hydrazonoethyl)benzene-1,3-diol (*Probe-1*) is in equilibrium between the non-fluorescent benzenoid structure and non-fluorescent quinoid one [57]. Fluorescence quenching of *Probe-1* was ascribed to the excited state intramolecular proton transfer (ESIPT) that can be blocked by deprotonation at higher pHs (Scheme 2). Hence, *Probe-1* can be used for detecting higher pHs. Also, the structure of *Probe-1* due to the different heteroatoms is an appropriate for chelating with metal ions that can be translated to optical responses.

Insert here Scheme 2

### 3.2. Influence of pH on the absorption and fluorescence spectra of Probe-1

As is shown in Figure 1A, the maximal absorbance of Probe-1 between 300 and 430 nm is centered at 374 nm, which is due to the typical for compounds of similar nature  $\pi \rightarrow \pi^*$  transition [70]. In acid medium the absorption character of the compound retains approximately the same. Conversely, in alkaline medium the absorption maximum is red shifted to 420 nm with a pronounced increase in the molar extinction coefficient, indicating the transition of the aromatic C-4 hydroxyl group to a phenolic anion and its conversion into dianion in a quinoidal form (Scheme 2). It should be noted that Probe-1 and its acidic solution did not exhibit a fluorescent emission (Figure 1B) which can be related to the existing ESIPT process. In basic environment Probe-1 exists in a quinoid form. Therefore the ESIPT process is not possible, so the fluorescence emission of the probe becomes feasible (Figure 1B).

Insert here Figure 1A and Figure 1B

These observations disclosed capability of the examined compound to work as a molecular probe for high pH values. That is why we performed a complete pH titration of Probe-1. The titration was started from high pH to assert the presence of the probe in the fluorescent dianion quinoid form.

Figure 2 illustrates the effect of the pH titration on the absorption of the probe. At pH 13.4, the probe exhibits absorption peaks centered at 310 nm ( $\epsilon = 6.1 \times 10^4 \text{ L}\cdot\text{mol}^{-1}\cdot\text{cm}^{-1}$ ) and 420 nm ( $\epsilon = 1.4 \times 10^4 \text{ L}\cdot\text{mol}^{-1}\cdot\text{cm}^{-1}$ ). In decreasing the pH till pH  $\approx 11$  no significant change was observed in the absorption spectrum. After pH  $\approx 11$  and till near pH  $\approx 10$ ; the absorbance at 420 nm sharply decreases and is hypsochromically shifted to 380 nm, the absorbance at 310 nm sharply decreases as well and a new absorption band centered at 270 nm appears. After pH  $\approx 10$  and till near pH  $\approx 2$  the absorbance at 420 nm does not change significantly, and then begins to increase again with a decrease in pH. The absorbance at 310 nm and 270 nm are caused by  $n \rightarrow \pi^*$  transitions in the anion and neutral forms of Probe-1, respectively. The high absorption and bathochromic shifts after pH near 2 are attributed to formation of a quinoid structure induced by protonation of the imine nitrogen (Scheme 3).

**Insert here Figure 2**

**Insert here Scheme 3**

Using the absorption changes of Probe-1 at 420 nm in pH range 9.3-10.7 (Inset of Figure 2) the  $pK_a$  value of 10.37 for the transformation from monophenolate to keto-hydrazine dianion form was calculated according to Eq. (1), where  $A_{max}$  and  $A_{min}$  are the maximum and minimum absorbance at 420 nm, respectively,  $A$  is the absorbance at the given pH value [71].

**Insert here Equation (1)**

On the other side, the fluorescence emission is high at higher pH values till near pH 12.5 and decreases significantly after pH  $\approx$  12.5. After pH  $\approx$  9.5, the fluorescence intensity becomes constant unaffected by decreasing the pH (Figure 3). The low fluorescence after pH  $\approx$  2, although the probe is in its quinoid form (Scheme 3), is attributed to quenching caused by ESIPT process.

**Insert here Figure 3**

Using the fluorescence changes of Probe-1 at 500 nm in pH range 9.6-12.5 (Inset of Figure 3) the  $pK_a$  value of 10.40 for the transformation from monophenolate to keto-hydrazine dianion form was calculated according to Eq. (2), where  $F_{max}$  and  $F_{min}$  are the maximum and minimum fluorescence intensity at 500 nm, respectively,  $F$  is the fluorescence intensity at the given pH value [72]. The  $pK_a$  value of 10.40 is near to that obtained by the absorption.

**Insert here Equation (2)**

### 3.3. *Influence of metal cations on the absorption and fluorescence of Probe-1*

The signaling behavior of Probe-1 towards a wide range of representative transition metal ions ( $Co^{2+}$ ,  $Cu^{2+}$ ,  $Fe^{3+}$ ,  $Cr^{3+}$ ,  $Ni^{2+}$ ,  $Pb^{2+}$ ,  $Cd^{2+}$ ,  $Zn^{2+}$ ,  $Hg^{2+}$  and  $Ag^+$  (as nitrate)) was studied in an aqueous solution (ethanol:water = 1:1, v/v) at pH = 10 (borate buffer) to assert the presence

of the probe in its fluorescent form. The influence of the cations was studied at low amount (one equivalent) and at high amount (ten equivalents) of the cations.

The photophysical behavior of Probe-1 as a function of metal ion concentration up to  $3 \times 10^{-4}$  mol L<sup>-1</sup> (10 equivalents) to  $3 \times 10^{-5}$  mol L<sup>-1</sup> solution of the probe was also examined at pH= 7.2 (HEPES buffer), however, no changes were observed. This indicates that Probe-1 is inappropriate detector for metal ions in a neutral environment.

### 3.3.1. Influence on the absorption spectrum

In borate buffer (pH = 10), the probe exhibits two absorption peaks centered at 310 nm ( $\epsilon = 1.1 \times 10^4$  L·mol<sup>-1</sup>·cm<sup>-1</sup>) and 420 nm ( $\epsilon = 4.2 \times 10^3$  L·mol<sup>-1</sup>·cm<sup>-1</sup>). As shown in Figure 4A, after addition of one equivalent of the cations, the absorption at 420 nm was not affected significantly by any of the cations under study, except Pb<sup>2+</sup> that causes a little increase of 32%. In the same time, Cu<sup>2+</sup> causes a little decrease in the absorbance at 420 nm by 12 %. However, after the addition of ten equivalents of cations, the effect of Pb<sup>2+</sup> and Cu<sup>2+</sup> becomes more pronounced 112% and -38%, respectively (Figure 4B).

**Insert here Figure 4AR1 and Figure 4BR1**

The increase in absorption at 420 nm by Pb<sup>2+</sup> ion is attributed to its binding to the quinoid form of the probe, thus shifting the equilibrium to the quinoid form that absorbs at 420 nm. In the other side, the decrease in absorption by Cu<sup>2+</sup> ion can be interpreted by its affinity to coordinate with the benzenoid form. So, the equilibrium is shifted to benzenoid form.

### 3.3.2. Influence on the emission spectrum

No pronounced effect on the fluorescence emission of Probe-1 at 500 nm after the excitation at 420 nm was observed by adding one equivalent of cations (Figure 5A). Using ten equivalents of the cations, only Cu<sup>2+</sup> caused a significant quenching (92%) (Figure 5B).

**Insert here Figure 5A and Figure 5B**

The quenching efficiency (*QE*) is calculated by Eq. (3), where  $F_0$  and  $F$  are the fluorescence intensity in the absence and presence of the quencher (Cu<sup>2+</sup>), respectively.

**Insert here Equation (3)**

The quenching of the fluorescence of Probe-1 in the presence of  $\text{Cu}^{2+}$  is ascribed to two factors: (i) The shifting of the equilibrium towards the non-fluorescent benzenoid form; (ii) The paramagnetism of  $\text{Cu}^{2+}$  that causes an energy transfer from probe to the cation [73]. The remarkable quenching only by excess of  $\text{Cu}^{2+}$  infers to the slow coordination between the probe and the  $\text{Cu}^{2+}$  ion.

Because of the slow coordination between the probe and  $\text{Cu}^{2+}$ , we studied the effect of the time on the probe response towards the presence of  $\text{Cu}^{2+}$ .

### 3.3.3. *Effect of time on the Probe-1 response in the presence of Cu(II)*

The response of Probe-1 towards  $\text{Cu}^{2+}$  as a function of the time was studied at different equivalents of  $\text{Cu}^{2+}$ .

When using one equivalent of  $\text{Cu}^{2+}$ , the decrease in absorption at 420 nm by time is slow (0.0031 per minute) and the equilibrium is reached after 30 minutes (Figure 6A). The decrease of emission at 500 nm was slow as well (223 A.U. per minute) and the saturation is achieved after 50 minutes (Figure 6B).

**Insert here Figure 6A and Figure 6B**

Using of 5 (Figure 7A) or 10 (Figure 7B) equivalents of  $\text{Cu}^{2+}$ , the saturation was achieved only after 3 minutes and faster quenching rates of fluorescence are observed.

**Insert here Figure 7A and Figure 7B**

The rate of decrease of both absorbance at 420 nm and emission at 500 nm of Probe-1 as well as the time of saturation at different equivalents of  $\text{Cu}^{2+}$  are summarized in Table 1.

**Insert here Table 1**

The increasing of the change rate in the absorption and emission spectra by excess of  $\text{Cu}^{2+}$  confirms the slow reaction between Probe-1 and  $\text{Cu}^{2+}$ , thus the equilibrium can be achieved either by long time or adding excess of  $\text{Cu}^{2+}$ .

#### 3.3.4. The sensitivity of Probe-1 to $\text{Cu}^{2+}$

Both the absorbance at 420 nm and the fluorescence intensity at 500 nm were decreased by increasing the concentration of  $\text{Cu}^{2+}$  (Figure 8, A and B).

**Insert here Figure 8A and Figure 8B**

From the titration plots of the absorption at 420 nm and the fluorescence intensity at 500 nm of Probe-1 against the concentration of  $\text{Cu}^{2+}$  (Insets of Figure 8A and Figure 8B), the linear range of sensitivity, correction coefficient  $\mathbf{R}^2$  and slope  $\mathbf{b}$  were determined. The standard deviation  $\sigma$  was calculated after measuring the absorption or fluorescence emission of the probe several times. The limit of detection was calculated from the formula  $\mathbf{LOD} = 3\sigma/\mathbf{b}$  [74] (Table 2).

**Insert here Table 2**

#### 3.3.5. Stoichiometric ratio of Probe-1/ $\text{Cu}^{2+}$ complex

The Job's plot analysis whether from the absorption spectra or from the fluorescence emission spectra (Figure 9), revealed a 2:1 stoichiometry for the complexation between the Probe-1 and  $\text{Cu}^{2+}$ , respectively.

**Insert here Figure 9A and Figure 9B**

The supposed binding mechanism in accordance to the similar chemical structures [75] is illustrated on Scheme 4.

**Insert here Scheme 4**

The binding constant of the Probe-1/Cu<sup>2+</sup> complex was evaluated from the titration plot of the fluorescence at 500 nm ( $\lambda_{\text{ex}} = 420$  nm) against the concentration of Cu<sup>2+</sup> (Insets of Figure 8B) using Benesi-Hildebrand Eq. (4), where  $I_o$  and  $I_\infty$  are emission intensities of the free and fully bound (saturation point) forms of Probe-1, respectively,  $I$  is emission intensity of the probe in the presence of Cu<sup>2+</sup> in known concentration,  $n$  represents the stoichiometry of binding of the probe to Cu<sup>2+</sup>,  $K$  is the binding constant of the probe to the Cu<sup>2+</sup> and  $[C]$  is the concentration of Cu<sup>2+</sup> [76].

**Insert here Equation (4)**

In substituting into Eq. (4) using  $n = \text{Probe-1/Cu}^{2+} = 2:1$ , the binding constant was found to be  $3 \times 10^9 \text{ M}^{-2}$ .

### 3.3.6. Selectivity of Probe-1 to Cu<sup>2+</sup>

The effect of the interfering cations on the Probe-1 response towards Cu<sup>2+</sup> was examined by measuring the absorption and fluorescence intensity of the probe in medium of Cu<sup>2+</sup> and the corresponding interfering cation. It is found that when Cu<sup>2+</sup> presents in concentrations higher than one equivalent, the interfering cation do not affect significantly on the fluorescence emission at 500 nm. At the same time, there is a significant influence on the absorption mode at 420 nm by Fe<sup>3+</sup> and Pb<sup>2+</sup>, which is expressed in an increase in the absorbance at 420 nm with 174% and 225% caused by Fe<sup>3+</sup> and Pb<sup>2+</sup>, respectively (Figure 10). The effect by Fe<sup>3+</sup> and Pb<sup>2+</sup> was ascribed to the affinity of the probe to coordinate also with Fe<sup>3+</sup> or Pb<sup>2+</sup> in addition to Cu<sup>2+</sup>.

**Insert here Figure 10A and Figure 10B**

However, in the presence of lower amount (one equivalent) of Cu<sup>2+</sup>, when the binding with the probe is slow, a strong interfering effect by Hg<sup>2+</sup> and Ag<sup>+</sup> on the probe's fluorescent response is observed. Hg<sup>2+</sup> accelerates the decreasing rate of the absorption of Probe-1 and its emission output (Figure 11). The higher decrease in the absorption and emission responses towards Cu<sup>2+</sup> in the presence of Hg<sup>2+</sup> was ascribed to the similar behavior of Hg<sup>2+</sup> and Cu<sup>2+</sup> in coordination with the benzenoid form.

**Insert here Figure 11A and Figure 11B**

Studying the effect of  $\text{Ag}^+$  (1 equivalent) on the absorption and emission response of Probe-1 towards the presence of  $\text{Cu}^{2+}$  (1 equivalent), it is observed that in the presence of  $\text{Ag}^+$ , the absorption at 420 nm is increased sharply after one minute, then begins to decrease in rate 0.018 per minute and does not decrease under the value of the probe itself even after 17 minutes (Figure 12). In the contrary, in the absence of  $\text{Ag}^+$ , the absorption at 420 nm decreases to 45% after 17 minutes. On the other hand, in the presence of  $\text{Ag}^+$ , the emission at 500 nm decreases in rate 582 A.U. per minute by 75% after 15 minute, but in the absence of  $\text{Ag}^+$ , the rate of quenching is 223 A.U. per minute and the quenching efficiency is 31% after 15 minutes.

**Insert here Figure 12A and Figure 12B**

The low decrease rate of the absorption at 420 nm in the presence of  $\text{Ag}^+$  is attributed to the coordination of  $\text{Ag}^+$  with the quinoid form of Probe-1 that competes with  $\text{Cu}^{2+}$  coordinating with the benzenoid form of the probe. On the other hand, the higher rate of fluorescence quenching is probably due to the energy transfer from Probe-1 to  $\text{Ag}^+$ .

**3.4. Influence of anions on the absorption and fluorescence of Probe-1**

No significant effect on the absorption and emission spectra of Probe-1 is observed by any of the anions under the study (including  $\text{F}^-$ ,  $\text{SO}_4^{2-}$ ,  $\text{HSO}_4^-$ ,  $\text{NO}_2^-$ ,  $\text{S}_2\text{O}_5^{2-}$ ,  $\text{CH}_3\text{COO}^-$ ,  $\text{CO}_3^{2-}$ ,  $\text{CN}^-$ ,  $\text{S}^{2-}$ ,  $\text{Br}^-$ ,  $\text{H}_2\text{PO}_4^-$  and  $\text{P}_2\text{O}_7^{4-}$ ), whether at one equivalent or at ten equivalents of anions.

**3.4.1. Influence of anions on Probe-1/ $\text{Cu}^{2+}$  complex**

The addition of any of the anions under study to Probe-1/ $\text{Cu}^{2+}$  complex did not affect both absorption and fluorescence spectra of the complex, with the exception of  $\text{S}^{2-}$ ,  $\text{H}_2\text{PO}_4^-$  and  $\text{P}_2\text{O}_7^{4-}$  that caused fluorescence enhancements by 143%, 97% and 134%, respectively (Figure 13A). On the other hand, the absorbance at 420 nm was increased significantly (131%) only by  $\text{S}^{2-}$  (Figure 13B).

**Insert here Figure 13AR1 and Figure 13BR1**

The increase in the absorption at 420 nm and the fluorescence at 500 nm caused by  $S^{2-}$  can be attributed to the de-metallization of the Probe-1/ $Cu^{2+}$  complex liberating the Probe-1 as a free and forming the covellite copper sulfide (CuS) nanoparticles that are responsible for the strong absorbance at 420 nm [77] (Scheme 5).

**Insert here Scheme 5**

The increase in the fluorescence emission without change in the absorption by phosphate and pyrophosphate anions can be attributed to the coordination of phosphate or pyrophosphate anions around  $Cu^{2+}$  in the Probe-1/ $Cu^{2+}$  complex thus decreasing the efficiency of fluorescence quenching by energy transfer from ligand to the  $Cu^{2+}$  ion.

The above indicates that Probe-1/ $Cu^{2+}$  complex could serve as a highly sensitive sensor for  $S^{2-}$  anions in absorption mode. From the plotting of the absorption at 420 nm against the concentration of  $S^{2-}$  (Figure 14), the linear range of sensitivity was found to be 0-30  $\mu M$ , correction coefficient  $R^2 = 0.914$ , a slope  $b$  was  $0.0011 \times 10^6 M^{-1}$ . The standard deviation  $\sigma$  was calculated to be 0.00361 and the limit of detection was calculated to be 10  $\mu M$ .

**Insert here Figure 14**

### 3.5. Logic gates by Probe-1

Thanks to the substantial changes in the absorption and fluorescence of Probe-1 in the presence of protons, hydroxide,  $Cu^{2+}$ ,  $S^{2-}$  and  $Pb^{2+}$ , it would be able to act as a multifunctional logic device. Using  $H^+$  and  $HO^-$  as inputs, the XOR and INHIBIT logic gates based on the absorption and emission output of Probe-1 were executed. Considering at the start point pH = 7 (coded as **00** for the inputs  $H^+$  and  $HO^-$ ), the absorbance of the probe at 420 nm and the fluorescence emission at 500 nm ( $\lambda_{ex} = 420$  nm) were lower than the threshold barrier (coded as **0** for output). Input  $H^+$  or  $HO^-$  ( $10^{-1}$  mol  $L^{-1}$ ) alone increased the absorbance at 420 nm and brought it to be higher than the threshold barrier (coded as **1** for output), however the fluorescence emission was increased only by input  $HO^-$  to be higher than the threshold barrier. The simultaneous inputs of  $H^+$  and  $HO^-$  annihilated each other and generated the initial low states (Figure 15). The behaviors of the absorbance at 420 nm (Figure 15A) and the fluorescence

emission at 500 nm (Figure 15B) mimic the *XOR* and *INHIBIT* logic gates using  $H^+$  and  $OH^-$  as inputs (Table 3).

**Insert here Figure 15A and Figure 15B**

**Insert here Table 3**

Furthermore, in alkaline solutions (pH 10) using  $Cu^{2+}$  and  $Pb^{2+}$  as chemical inputs, *IMPLICATION*, *TRANSFER* and *NOT TRANSFER* gates were achieved. As is shown in Figure 16 and Table 4, the presence of input  $Cu^{2+}$  decreases the absorbance at 420 nm but the presence of input  $Pb^{2+}$  increases this absorbance whatever it is alone or mixed with  $Cu^{2+}$ . Considering the barrier level of the absorbance at 420 nm is higher than that by input  $Cu^{2+}$  alone but in the same time is lower than that by the Probe-1 alone, the behavior of the absorbance at 420 nm mimics *IMPLICATION* logic gate (Figure 16A, threshold A). However, considering the barrier level is higher than the absorbance of Probe-1 alone, the absorbance changes at 420 nm mimic *TRANSFER* logic gate (Figure 16A, threshold B). On the other hand, the fluorescence emission of the system is lower than the barrier level only in the presence of  $Cu^{2+}$  whether it is alone or mixed with  $Pb^{2+}$  and this fluorescence behavior mimics *NOT TRANSFER* logic gate (Figure 16B).

**Insert here Figure 16A and Figure 16B**

**Insert here Table 4**

Also, using  $Cu^{2+}$  and  $S^{2-}$  as chemical inputs and the absorption of Probe-1 as output, AND logic gate at molecular scale could be constructed. Monitoring the absorbance at 420 nm and considering the absorbance of the probe alone is in a low state (coded **0** for output), the presence of any of the inputs alone remains the absorbance lower than the threshold. However, the presence of the two inputs together increases the absorbance at 420 nm and brought it to be higher than the threshold (coded as 1 for output) (Figure 17). Such behavior is very well correlated with *AND* logic gate (Table 5).

**Insert here Figure 17**

Insert here Table 5

#### 4. Conclusions

In the present work we report the preparation of (*E*)-4-(1-hydrazonoethyl)benzene-1,3-diol (Probe-1) in an improved synthetic procedure as well as the results of the detailed examination of its photophysical characteristics as a function of pH of the medium and the presence of a wide range of representative transition metal ions and anions. As a result of the ESIPT process and equilibrium between the non-fluorescent benzenoid structure and the non-fluorescent quinoid one Probe-1 has a high potential for use as a molecular sensor in an alkaline environment. Furthermore, Probe-1 is capable of selectively recognizing  $\text{Cu}^{2+}$  ions in the environment in concentrations higher than one equivalent (LOD = 3  $\mu\text{M}$ ), forming a complex in a 2:1 ratio. At the same time, the Probe-1/ $\text{Cu}^{2+}$  complex itself serves as a highly sensitive molecular sensor for  $\text{S}^{2-}$  anions in absorption mode (LOD = 10  $\mu\text{M}$ ) due to its de-metallization to covellite copper sulfide (CuS) nanoparticles. Finally, it has been shown that Probe-1 is capable of executing many different logic gates such as *XOR*, *AND*, *INHIBIT*, *IMPLICATION*, *TRANSFER* and *NOT TRANSFER*.

#### Acknowledgements

This work was supported by the Science Foundation at the University of Chemical Technology and Metallurgy (Sofia, Bulgaria) – project No 11811/2018 and project No 11818/2018. Authors also acknowledge the Science foundation of Assiut University (Assiut, Egypt).

## References

- [1] O. Young, R. Thomson, V. Merhtens, M. Loeffen, Industrial application to cattle of a method for the early determination of meat ultimate pH, *Meat. Sci.* 67 (2004) 107-112.
- [2] N. Georgiev, A. Said, R. Toshkova, R. Tzoneva, V. Bojinov, A novel water-soluble perylenetetracarboxylic diimide as a fluorescent pH probe: chemosensing, biocompatibility and cell imaging, *Dyes Pigments* 160 (2019) 28-36.
- [3] Z.-Q. Hu, M. Li, M.-D. Liu, W.-M. Zhuang, G.-K. Li, A highly sensitive fluorescent acidic pH probe based on rhodamine B diethyl-2-aminobutenedioate conjugate and its application in living cells, *Dyes Pigments* 96 (2013) 71-75.
- [4] W. Jin, J. Jiang, X. Wang, X. Zhu, G. Wang, Y. Song, C. Ba, Continuous intra-arterial blood pH monitoring in rabbits with acid-base disorders, *Respir. Physiol. Neurobiol.* 177 (2011) 183-188.
- [5] S. Grant, K. Bettencourt, P. Krulevitch, J. Hamilton, R. Glass, In vitro and in vivo measurements of fiber optic and electrochemical sensors to monitor brain tissue pH, *Sensors Actuators B: Chem.* 72 (2001) 174-179.
- [6] R. Bryaskova, N. Georgiev, S. Dimov, R. Tzoneva, C. Detrembleur, A. Asiri, K. Alamry, V. Bojinov, Novel nanosized water soluble fluorescent micelles with embedded perylene diimide fluorophores for potential biomedical applications: cell permeability, localization and cytotoxicity, *Mater. Sci. Eng. C* 51 (2015) 7-15.
- [7] X. Zhang, H. Jiang, J. Jin, X. Xu, Q. Zhang, Analysis of acid rain patterns in northeastern China using a decision tree method, *Atmos. Environ.* 46 (2012) 590-596.
- [8] N. Georgiev, A. Said, R. Toshkova, R. Tzoneva, V. Bojinov, A novel water-soluble perylenetetracarboxylic diimide as a fluorescent pH probe: chemosensing, biocompatibility and cell imaging, *Dyes Pigments* 160 (2019) 28-36.
- [9] M. Shamsipur, F. Abbasitabar, V. Zare-Shahabadi, Shahabadi, M. Akhond, Broad-range optical pH sensor based on binary mixed-indicator doped sol-gel film and application of artificial neural network, *Anal. Lett.* 41 (2008) 3113-3123.
- [10] A. de Silva, B. McCaughan, B. McKinney, M. Querol, Newer optical-based molecular devices from older coordination chemistry, *Dalton Trans.* 10 (2003) 1902-1938.
- [11] V. Bojinov, N. Georgiev, Molecular sensors and molecular logic gates, *J. Univ. Chem. Tech. Metall.* 46 (2011) 3-26.

- [12] D. Wencel, T. Abel, C. McDonagh, Optical chemical pH sensors, *Anal. Chem.* 86 (2014) 15-29.
- [13] J. Callan, A. de Silva, D. Magri, Luminescent sensors and switches in the early 21st century, *Tetrahedron* 61 (2005) 8551-8588.
- [14] N. Georgiev, A. Sakr, V. Bojinov, Design and synthesis of a novel PET and ICT based 1,8-naphthalimide-FRET bichromophore as a four-input Disabled-Enabled-OR logic gate, *Sensors Actuators B: Chem.* 221 (2015) 625-634.
- [15] Z. Liu, F. Luo, T. Chen, Phenolphthalein immobilized membrane for an optical pH sensor, *Anal. Chim. Acta* 510 (2004) 189-194.
- [16] M. Sotomayor, M.-A. De Paoli, W. de Oliveira, Fiber-optic pH sensor based on Poly(o-methoxyaniline), *Anal. Chim. Acta* 353 (1997) 275-280.
- [17] N. Georgiev, V. Bojinov, P. Nikolov, Design and synthesis of a novel pH sensitive core and peripherally 1,8-naphthalimide-labeled PAMAM dendron as light harvesting antenna, *Dyes Pigments* 81 (2009) 18-26.
- [18] S. Draxler, M. Lippitsch, pH sensors using fluorescence decay time. *Sensors Actuators B: Chem.* 29 (1995) 199-203.
- [19] N. Georgiev, M. Dimitrova, Y. Todorova, V. Bojinov, Synthesis, chemosensing properties and logic behaviour of a novel ratiometric 1,8-naphthalimide probe based on ICT and PET, *Dyes Pigments* 131 (2016) 9-17.
- [20] S. Dimov, N. Georgiev, A. Asiri, V. Bojinov, Synthesis and sensor activity of a PET-based 1,8-naphthalimide probe for  $Zn^{2+}$  and pH determination, *J. Fluoresc.* 24 (2014) 1621-1628.
- [21] D. Aigner, B. Ungerböck, T. Mayr, R. Saf, I. Klimant, S. Borisov, Fluorescent materials for pH sensing and imaging based on novel 1,4-diketopyrrolo-[3,4-c]pyrrole dyes. *J. Mater. Chem. C* 1 (2013) 5685-5693.
- [22] K. Alamry, N. Georgiev, S. Abdullah El-Daly, L. Taib, V. Bojinov, A highly selective ratiometric fluorescent pH probe based on a PAMAM wavelength-shifting bichromophoric system, *Spectrochim. Acta A: Mol. Biomol. Spectrosc.* 135 (2015) 792-800.
- [23] R. Uauy, M. Olivares, M. Gonzalez, Essentiality of copper in humans, *Am. J. Clin. Nutr.* 67 (1998) 952S-967S.
- [24] E. Maryon, S. Molloy, A. Zimnicka, J. Kaplan, Copper entry into human cells: progress and unanswered questions, *BioMetals* 20 (2007) 355-364.

- [25] M. Turski, D. Thiele, New roles for copper metabolism in cell proliferation, signaling, and disease, *J. Biol. Chem.* 284 (2009) 717-721.
- [26] K. Barnham, C. Masters, A. Bush, Neurodegenerative diseases and oxidative stress, *Nat. Rev. Drug Discov.* 3 (2004) 205-214.
- [27] B. Sarkar, Treatment of Wilson and Menkes diseases, *Chem. Rev.* 99 (1999) 2535-2544.
- [28] V. Bojinov, N. Georgiev, P. Bosch, Design and synthesis of highly photostable yellow-green emitting 1,8-naphthalimides as fluorescent sensors for metal cations and protons, *J. Fluoresc.* 19 (2009) 127-139.
- [29] D. Quang, J. Kim, Fluoro- and chromogenic chemodosimeters for heavy metal ion detection in solution and biospecimens, *Chem. Rev.* 110 (2010) 6280-6301.
- [30] X. Chen, T. Pradhan, F. Wang, J. Kim, J. Yoon, Fluorescent chemosensors based on spiroring-opening of xanthenes and related derivatives, *Chem. Rev.* 112 (2012) 1910-1956.
- [31] V. Bojinov, I. Panova, J.-M. Chovelon, Novel blue emitting tetra- and pentamethylpiperidin-4-yloxy-1,8-naphthalimides as photoinduced electron transfer based sensors for transition metal ions and protons, *Sensors Actuators B: Chem.* 135 (2008) 172-180.
- [32] L. Tang, M. Cai, A highly selective and sensitive fluorescent sensor for  $\text{Cu}^{2+}$  and its complex for successive sensing of cyanide via  $\text{Cu}^{2+}$  displacement approach, *Sensors Actuators B: Chem.* 173 (2012) 862-867.
- [33] M. Kumar, N. Kumar, V. Bhalla, P. Sharma, T. Kaur, Highly selective fluorescence turn-on chemodosimeter based on rhodamine for nanomolar detection of copper ions, *Org. Lett.* 14 (2012) 406-409.
- [34] V. Bojinov, N. Georgiev, N. Marinova, Design and synthesis of highly photostable fluorescence sensing 1,8-naphthalimide-based dyes containing s-triazine UV absorber and HALS units, *Sensors Actuators B: Chem.* 148 (2010) 6-16.
- [35] F.-J. Huo, J. Su, Y.-Q. Sun, C.-X. Yin, H.-B. Tong, Z.-X. Nie, A rhodamine-based dual chemosensor for the visual detection of copper and the ratiometric fluorescent detection of vanadium, *Dyes Pigments* 86 (2010) 50-55.
- [36] Y. Guo, Z. Wang, W. Qu, H. Shao, X. Jiang, Colorimetric detection of mercury, lead and copper ions simultaneously using protein-functionalized gold nanoparticles, *Biosens. Bioelectron.* 26 (2011) 4064-4069.

- [37] V. Bojinov, I. Panova, D. Simeonov, N. Georgiev, Synthesis and sensor activity of photostable blue emitting 1,8-naphthalimides containing s-triazine UV absorber and HALS fragments, *J. Photochem. Photobiol. A: Chem.* 210 (2010) 89-99.
- [38] N. Aksuner, E. Henden, I. Yilmaz, A. Cukurovali, A highly sensitive and selective fluorescent sensor for the determination of copper(II) based on a schiff base, *Dyes Pigments* 83 (2009) 211-217.
- [39] N. Georgiev, V. Bojinov, Design, synthesis and sensor activity of a highly photostable blue emitting 1,8-naphthalimide, *J. Lumin.* 132 (2012) 2235-2241.
- [40] X.-J. Hu, C.-M. Li, X.-Y. Song, D. Zhang, Y.-S. Li, A new Cu<sup>2+</sup> selective self-assembled fluorescent chemosensor based on thiacalix[4]arene, *Inorg. Chem. Commun.* 14 (2011) 1632-1635.
- [41] K. Ko, J.-S. Wu, H. Kim, P. Kwon, J. Kim, R. Bartsch, J. Lee, J. Kim, Rationally designed fluorescence 'turn-on' sensor for Cu<sup>2+</sup>, *Chem. Commun.* 47 (2011) 3165-3167.
- [42] N. Georgiev, M. Dimitrova, A. Mavrova, V. Bojinov, Synthesis, fluorescence-sensing and molecular logic of two water-soluble 1,8-naphthalimides, *Spectrochim. Acta Part A* 183 (2017) 7-16.
- [43] A. Said, N. Georgiev, V. Bojinov, Synthesis of a single 1,8-naphthalimide fluorophore as a molecular logic lab for simultaneously detecting of Fe<sup>3+</sup>, Hg<sup>2+</sup> and Cu<sup>2+</sup>, *Spectrochim. Acta A: Mol. Biomol. Spectrosc.* 196 (2018) 76-82.
- [44] L. Tang, P. Zhou, Q. Zhang, Z. Huang, J. Zhao, M. Cai, A simple quinoline derivatized thiosemicarbazone as a colorimetric and fluorescent sensor for relay recognition of Cu<sup>2+</sup> and sulfide in aqueous solution, *Inorg. Chem. Commun.* 36 (2013) 100-104.
- [45] Hydrogen Sulfide, Environmental Health Criteria, No.19, World Health Organization, Geneva, 1981.
- [46] X. Cao, W. Lin, L. He, A near-infrared fluorescence turn-on sensor for sulfide anions, *Org. Lett.* 13 (2011) 4716-4719.
- [47] Y. Liu, P. Liang, L. Guo, Nanometer titanium dioxide immobilized on silica gel as sorbent for preconcentration of metal ions prior to their determination by inductively coupled plasma atomic emission spectrometry, *Talanta* 68 (2005) 25-30.
- [48] A. Ensafi, T. Khayamian, A. Benvidi, E. Mirmomtaz, Simultaneous determination of copper, lead and cadmium by cathodic adsorptive stripping voltammetry using artificial neural network, *Anal. Chim. Acta* 561 (2006) 225-232.

- [49] A. Gonzales, M. Firmino, C. Nomura, F. Rocha, P. Oliveira, I. Gaubeur, Peat as a natural solid-phase for copper preconcentration and determination in a multicommutated flow system coupled to flame atomic absorption spectrometry, *Anal. Chim. Acta* 636 (2009) 198-204.
- [50] S.-P. Wu, T.-H. Wang, S.-R. Liu, A highly selective turn-on fluorescent chemosensor for copper(II) ion, *Tetrahedron* 66 (2010) 9655-9658.
- [51] D. Maity, T. Govindaraju, Highly selective visible and near-IR sensing of  $\text{Cu}^{2+}$  based on thiourea-salicylaldehyde coordination in aqueous media, *Chem. Eur. J.* 17 (2011) 1410-1414.
- [52] H. Jung, P. Kwon, J.W. Lee, J.I. Kim, C. Hong, J.W. Kim, S. Yan, J.Y. Lee, J.H. Lee, T. Joo, J.S. Kim, Coumarin-derived  $\text{Cu}^{2+}$ -selective fluorescence sensor: synthesis, mechanisms, and applications in living cells, *J. Am. Chem. Soc.* 131 (2009) 2008-2012.
- [53] L. Yuan, W. Lin, B. Chen, Y. Xie, Development of FRET-based ratiometric fluorescent  $\text{Cu}^{2+}$  chemodosimeters and the applications for living cell imaging, *Org. Lett.* 14 (2012) 432-435.
- [54] A. Kumar, V. Kumar, U. Diwan, K. Upadhyay, Highly sensitive and selective naked-eye detection of  $\text{Cu}^{2+}$  in aqueous medium by a ninhydrin–quinoxaline derivative, *Sensors Actuators B: Chem.* 176 (2013) 420-427.
- [55] N. Li, Y. Xiang, X. Chen, A. Tong, Salicylaldehyde hydrazones as fluorescent probes for zinc ion in aqueous solution of physiological pH, *Talanta* 79 (2009) 327-332.
- [56] S. Sharma, M. Hundal, N. Singh, G. Hundal, Nanomolar fluorogenic recognition of Cu(II) in aqueous medium - A highly selective “on-off” probe based on mesitylene derivative, *Sensors Actuators B: Chem.* 188 (2013) 590-596.
- [57] A. Said, N. Georgiev, V. Bojinov, Sensor activity and logic behavior of dihydroxyphenyl hydrazone derivative as a chemosensor for  $\text{Cu}^{2+}$  determination in alkaline aqueous solutions, *J. Photochem. Photobiol. A: Chem.* 311 (2015) 16-24.
- [58] N. Georgiev, I. Yaneva, A. Surleva, A. Asiri, V. Bojinov, Synthesis, selective pH-sensing activity and logic behavior of highly water-soluble 1,8-naphthalimide and dihydroimidazonaphthalimide derivatives. *Sensors Actuators B: Chem.* 184 (2013) 54-63.
- [59] W. Jiang, H. Zhang, Y. Liu, Unimolecular half-adders and half-subtractors based on acid-base reaction, *Front. Chem. China* 4 (2009) 292-298.

- [60] N. Georgiev, M. Lyulev, V. Bojinov, Sensor activity and logic behavior of PET based dihydroimidazonaphthalimide diester, *Spectrochim. Acta A: Mol. Biomol. Spectrosc.* 97 (2012) 512-520.
- [61] N. Georgiev, S. Dimov, A. Asiri, K. Alamry, A. Obaid, V. Bojinov, Synthesis, selective pH-sensing activity and logic behavior of highly water-soluble 1,8-naphthalimide and dihydroimidazonaphthalimide derivatives, *J. Lumin.* 149 (2014) 325-332.
- [62] N. Georgiev, M. Lyulev, K. Alamry, S. El-Daly, L. Taib, V. Bojinov, Synthesis, sensor activity and logic behavior of a highly water-soluble 9,10-dihydro-7H-imidazo[1,2-*b*]benz[*d,e*]isoquinolin-7-one dicarboxylic acid, *J. Photochem. Photobiol. A: Chem.* 297 (2014) 31-38.
- [63] D. Margulies, G. Melman, A. Shanzler, Full-adder and full-subtractor, an additional step toward a molecular, *J. Am. Chem. Soc.* 128 (2006) 4865-4871.
- [64] M. Suresh, D. Jose, A. Das, [2,2'-Bipyridyl]-3,3'-diol as a molecular half-subtractor, *Org. Lett.* 9 (2007) 441-444.
- [65] S. Kumar, V. Luxami, R. Saini, D. Kaur, Superimposed molecular keypad lock and half-subtractor implications in a single fluorophore, *Chem. Commun.* 0 (2009) 3044-3046.
- [66] N. Kaur, S. Kumar, Aminoanthraquinone-based chemosensors: colorimetric molecular logic mimicking molecular trafficking and a set-reset memorized device, *Dalton Trans.* 41 (2012) 5217-5224.
- [67] S. Karmakar, S. Mardanya, P. Pal, S. Baitalik, Design of multichannel osmium-based metalloreceptor for anions and cations by taking profit from metal-ligand interaction and construction of molecular keypad lock and memory device, *Inorg. Chem.* 54 (2015) 11813-11825.
- [68] X.-J. Jiang, D.K.P. Ng, Sequential logic operations with a molecular keypad lock with four inputs and dual fluorescence outputs, *Angew. Chem. Int. Ed.* 53 (2014) 10481-10484.
- [69] C. Carvalho, Z. Dominguez, J. Silva, U. Pischel, A supramolecular keypad lock, *Chem. Commun.* 51 (2015) 2698-2701.
- [70] J. Liu, B. Wu, B. Zhang, Synthesis of  $\beta$ -cyclodextrin-2,4-dihydroxyacetophenone-phenylhydrazine and its application, *J. Chin. Chem. Soc.* 52 (2005) 1165-1170.
- [71] J. Qian, Y. Xu, X. Qian, S. Zhang, A pair of regio-isomeric compounds acting as molecular logic gates with different functions, *J. Photochem. Photobiol. A: Chem.* 207 (2009) 181-189.

- [72] L. Daffy, A. de Silva, H. Gunaratne, C. Huber, P. Lynch, T. Werner, O. Wolfbeis, Arenedicarboximide building blocks for fluorescent photoinduced electron transfer pH sensors applicable with different media and communication wavelengths, *Chem. Eur. J.* 4 (1998) 1810-1815.
- [73] Y. Xiang, Z. Li, X. Chen, A. Tong, Highly sensitive and selective optical chemosensor for determination of  $\text{Cu}^{2+}$  in aqueous solution, *Talanta* 74 (2008) 1148-1153.
- [74] M. Attia, A. Youssef, R. El-Sherif, Durable diagnosis of seminal vesicle and sexual gland diseases using the nano optical sensor thin film Sm-doxycycline complex, *Anal. Chim. Acta* 835 (2014) 56-64.
- [75] J. Costamagna, J. Vargas, R. Latorre, A. Alvarado, G. Mena, Coordination compounds of copper, nickel and iron with Schiff bases derived from hydroxynaphthaldehydes and salicylaldehydes, *Coord. Chem. Rev.* 119 (1992) 67-88.
- [76] Z.-B. Zheng, Y.-Q. Wu, K.-Z. Wang, F. Li, pH luminescence switching, dihydrogen phosphate sensing, and cellular uptake of a heterobimetallic ruthenium(II)-rhenium(I) complex, *Dalton Trans.* 43 (2014) 3273-3284.
- [77] S. K. Haram, A. R. Mahadeshwar and S. G. Dixit, Synthesis and characterization of copper sulfide nanoparticles in Triton-X 100 water-in-oil microemulsions, *J. Phy. Chem.* 100 (1996) 5868-5873.

## Tables

**Table 1**

Rate of decrease of emission and absorption of Probe-1 and time of saturation at different equivalents of  $\text{Cu}^{2+}$ .

Equivalents of $\text{Cu}^{2+}$	Absorption at 420 nm		Emission at 500 nm	
	Rate of decrease Per minute	Saturation time (minute)	Rate of decrease A.U. Per minute	Saturation time (minute)
One	0.0029	50	223	50
Five	0.022	3	3262	3
Ten	0.034	3	3427	3

**Table 2**

The linear range of sensitivity, correction coefficient, slope and the limit of detection (LOD) using absorbance at 420 nm and emission at 500 nm for Probe-1 toward  $[\text{Cu}^{2+}]$ .

	Linear range of detection ( $\mu\text{M}$ )	Correction coefficient ( $R^2$ )	Slope (b) ( $10^6 \text{ M}^{-1}$ )	Standard deviation ( $\sigma$ )	LOD ( $\mu\text{M}$ )
Absorption ( $A_{420}$ )	20-30	0.95685	-0.00689	0.0161	27
Emission ( $F_{500}$ )	0-30	0.97213	-443.49	557.48	3

**Table 3**

The truth table for logic behavior of Probe-1 using  $\text{H}^+$  and  $\text{HO}^-$  as chemical inputs

Chemical Inputs		Outputs	
Input 1	Input 2	Output 1	Output 2
$\text{H}^+$	$\text{OH}^-$	Absorbance ( $A_{420}$ )	Fluorescence ( $F_{500}$ )
0	0	0	0
0	1	1	1
1	0	1	0
1	1	0	0
Logic gate:		<b>XOR</b>	<b>INHIBIT (<math>\text{HO}^-</math>)</b>

**Table 4**

The truth table for logic behavior of Probe-1 using  $\text{Cu}^{2+}$  and  $\text{Pb}^{2+}$  as chemical inputs.

Chemical Inputs		Outputs		
Input 1	Input 2	Output 1	Output 2	Output 3
$\text{Cu}^{2+}$	$\text{Pb}^{2+}$	Absorbance ( $A_{420}$ ) <i>Level A</i>	Absorbance ( $A_{420}$ ) <i>Level B</i>	Fluorescence ( $F_{500}$ )
0	0	1	0	1
0	1	1	1	1
1	0	0	0	0
1	1	1	1	0
Logic gate:		<b><i>IMPLICATION</i></b>	<b><i>TRANSFER (<math>\text{Pb}^{2+}</math>)</i></b>	<b><i>NOT TRANSFER (<math>\text{Cu}^{2+}</math>)</i></b>

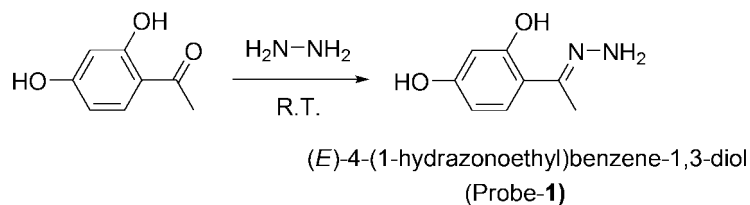
**Table 5**

The truth table for logic behavior of Probe-1 using  $\text{Cu}^{2+}$  and  $\text{S}^{2-}$  as chemical inputs.

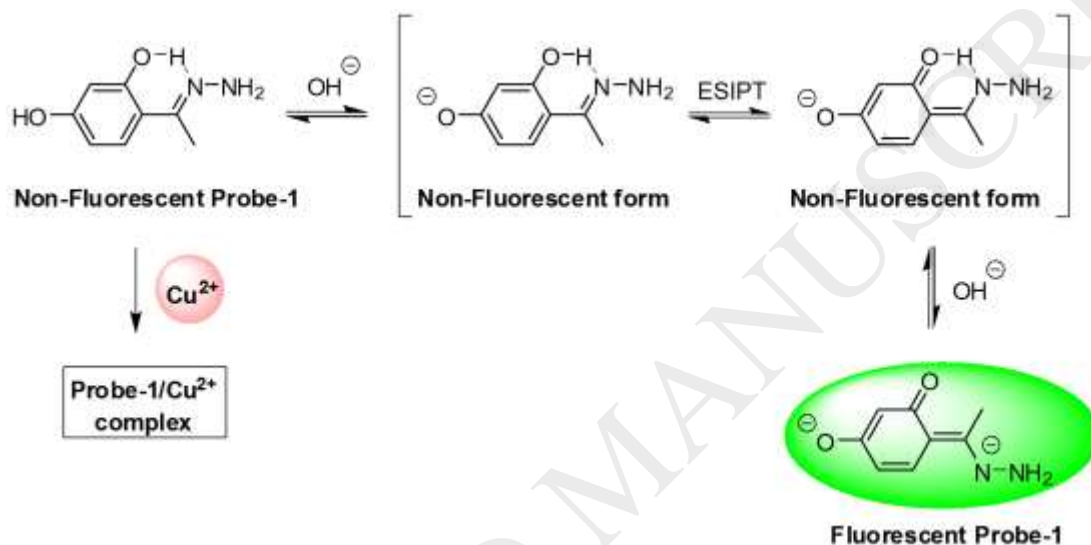
Input 1	Input 2	Output
$\text{Cu}^{2+}$	$\text{S}^{2-}$	Absorbance ( $A_{420}$ )
0	0	0
0	1	0
1	0	0
1	1	1
Logic gate:		<b><i>AND</i></b>

## Scheme Captions

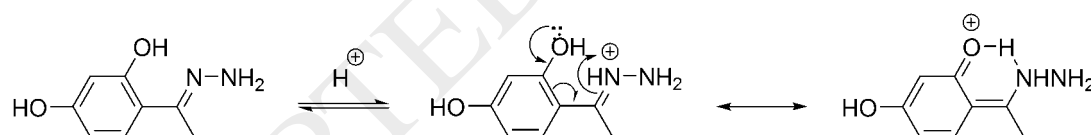
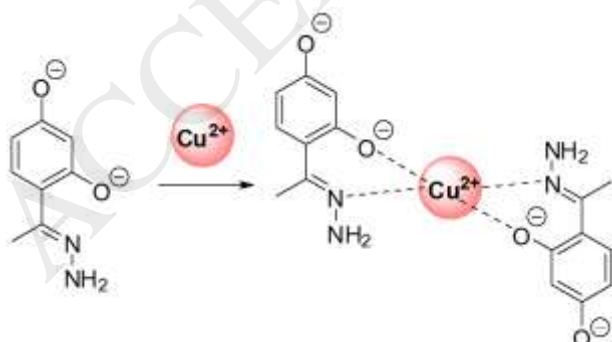
Scheme 1. Synthesis of Probe-1.

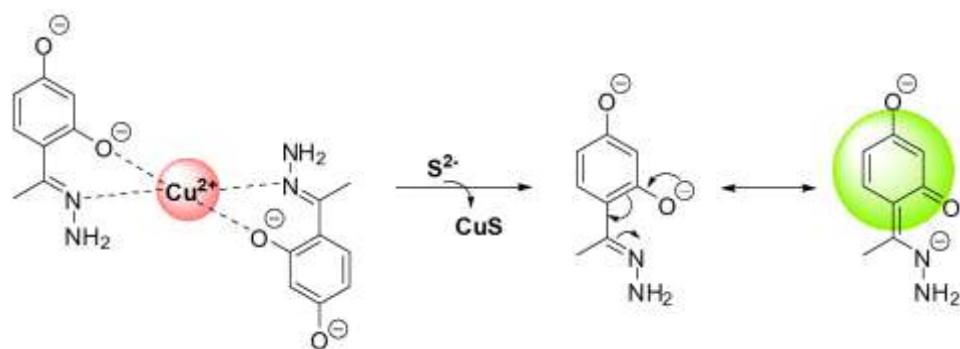


Scheme 2. Structural changes of Probe-1 in alkaline media.



Scheme 3. Structural transformation of Probe-1 in strong acid medium.

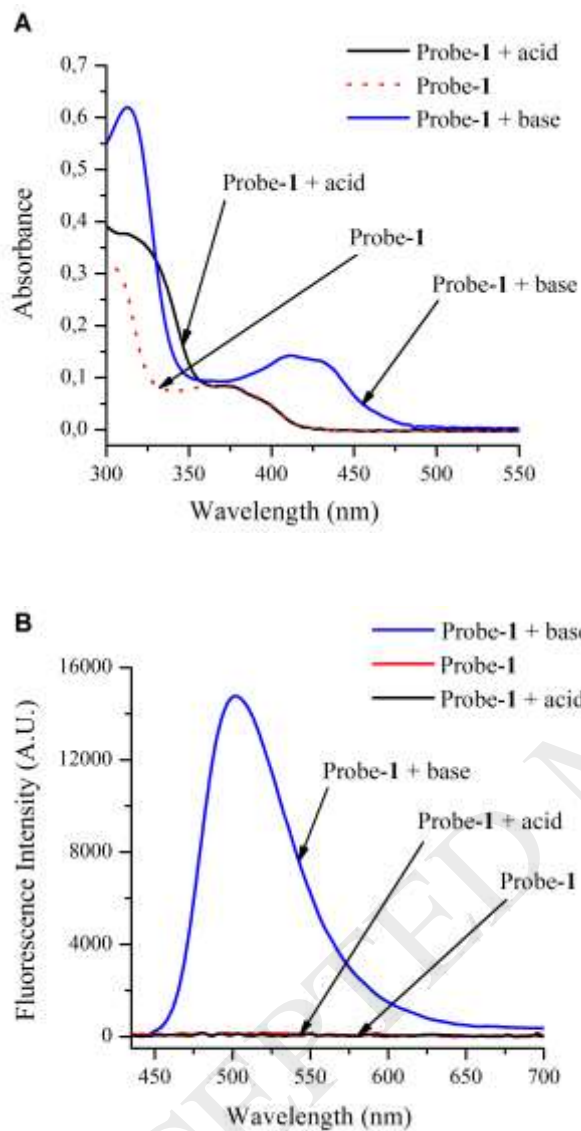
Scheme 4. Binding between Probe-1 and  $\text{Cu}^{2+}$  at pH=10 (borate buffer).Scheme 5. De-metallization of Probe-1/ $\text{Cu}^{2+}$  complex with  $\text{S}^{2-}$  anion.



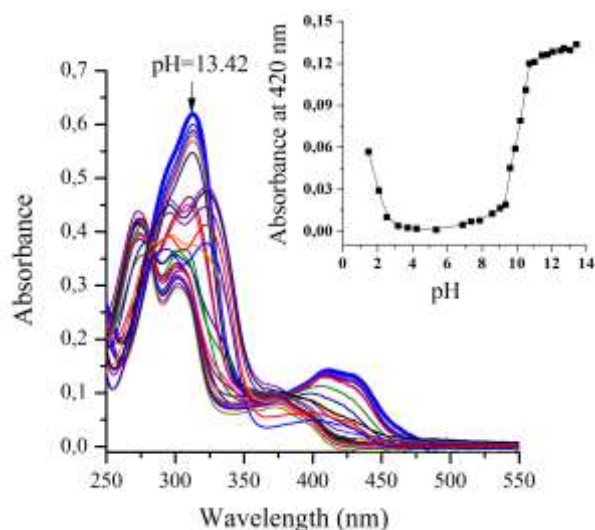
ACCEPTED MANUSCRIPT

## Figure Legends

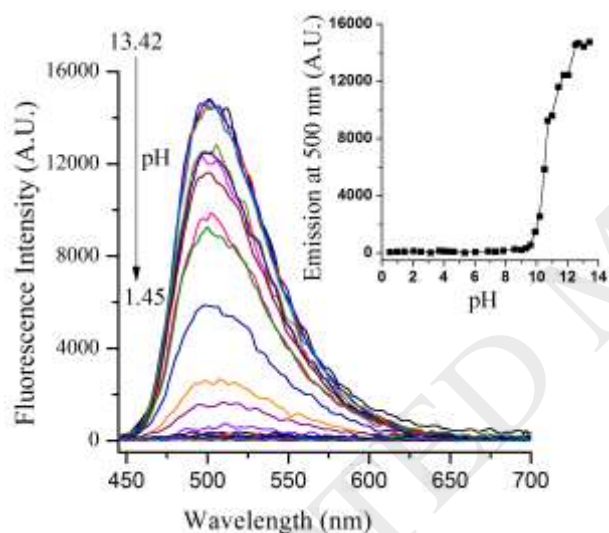
**Fig. 1.** Effect of acid and base on (A) absorption and (B) fluorescence ( $\lambda_{\text{ex}} = 420 \text{ nm}$ ) spectra of Probe-1 in aqueous solution.



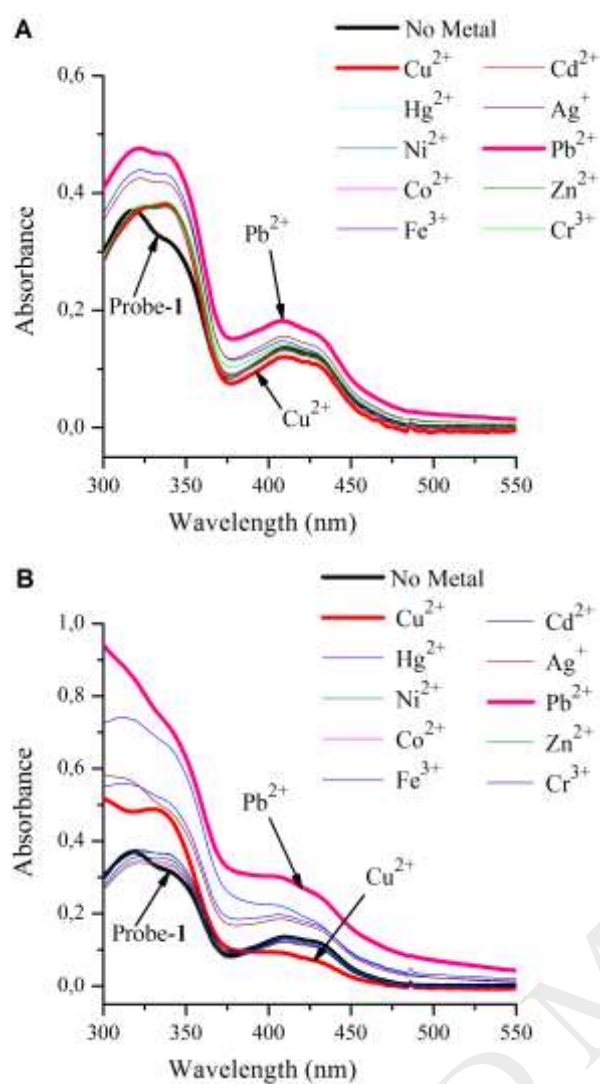
**Fig.2.** Effect of pH on the absorption spectrum of Probe-1 in ethanol/water (1:2, v/v) solution ( $C = 1 \times 10^{-5} \text{ mol L}^{-1}$ ). Inset: Absorbance of Probe-1 at 420 nm as a function of pH.



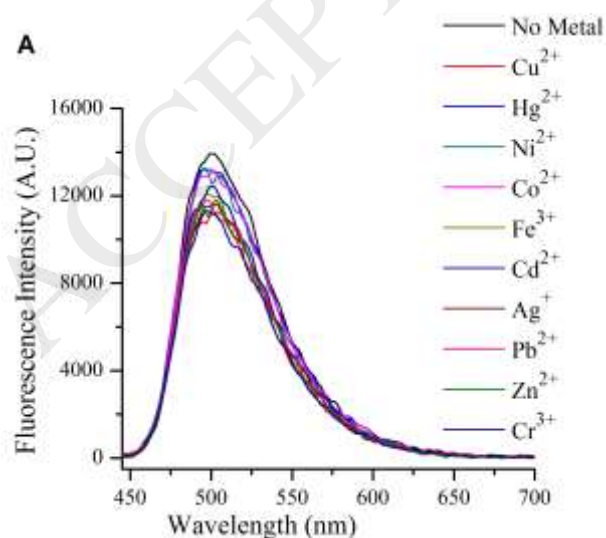
**Fig.3.** Effect of pH on the fluorescence spectrum of Probe-1 ( $\lambda_{\text{ex}} = 420 \text{ nm}$ ) in ethanol/water (1:2, v/v) solution ( $C = 1 \times 10^{-5} \text{ mol L}^{-1}$ ). Inset: Fluorescence of Probe-1 at 500 nm as a function of pH.

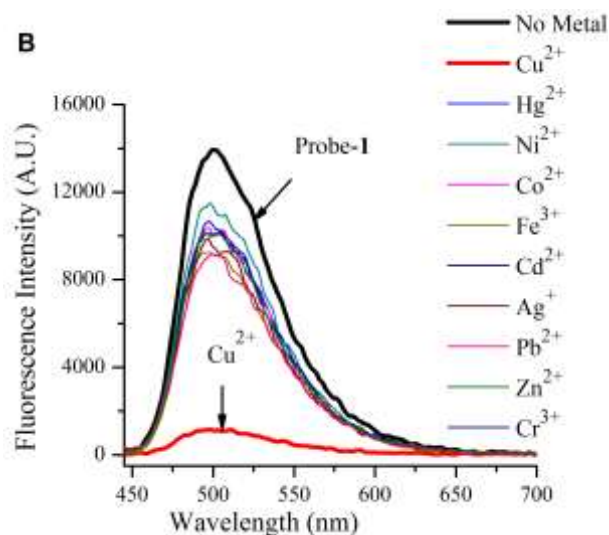


**Fig. 4.** Effect of (A) one equivalent ( $C = 3 \times 10^{-5} \text{ mol L}^{-1}$ ) and (B) ten equivalents ( $C = 3 \times 10^{-4} \text{ mol L}^{-1}$ ) of the cations on the absorption spectrum of Probe-1 in aqueous solution ( $C = 3 \times 10^{-5} \text{ mol L}^{-1}$ ) and borate buffer ( $C = 0.2 \text{ mol L}^{-1}$ , pH = 10).

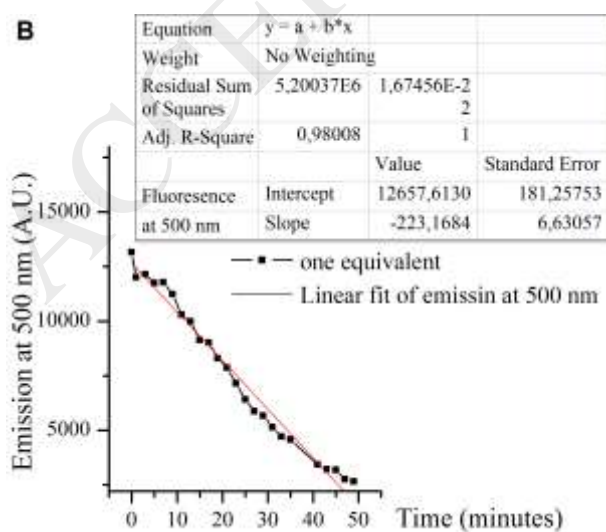
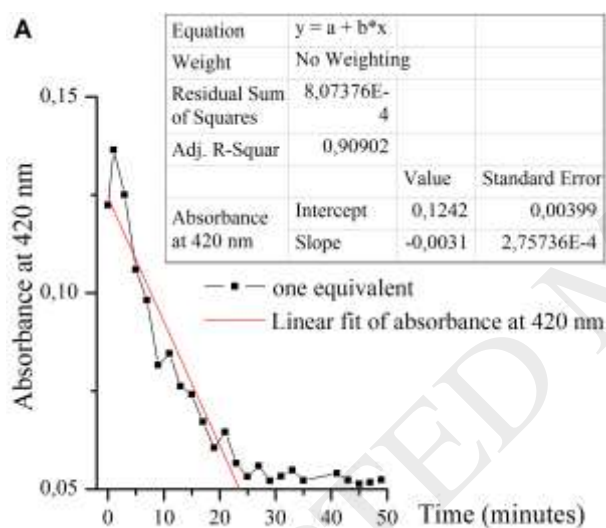


**Fig. 5.** Effect of (A) one equivalent ( $C = 3 \times 10^{-5} \text{ mol L}^{-1}$ ) and (B) ten equivalents ( $C = 3 \times 10^{-4} \text{ mol L}^{-1}$ ) of the cations on the fluorescence spectrum of Probe-1 ( $\lambda_{\text{ex}} = 420 \text{ nm}$ ) in aqueous solution ( $C = 3 \times 10^{-5} \text{ mol L}^{-1}$ ) and borate buffer ( $C = 0.2 \text{ mol L}^{-1}$ ,  $\text{pH} = 10$ ).

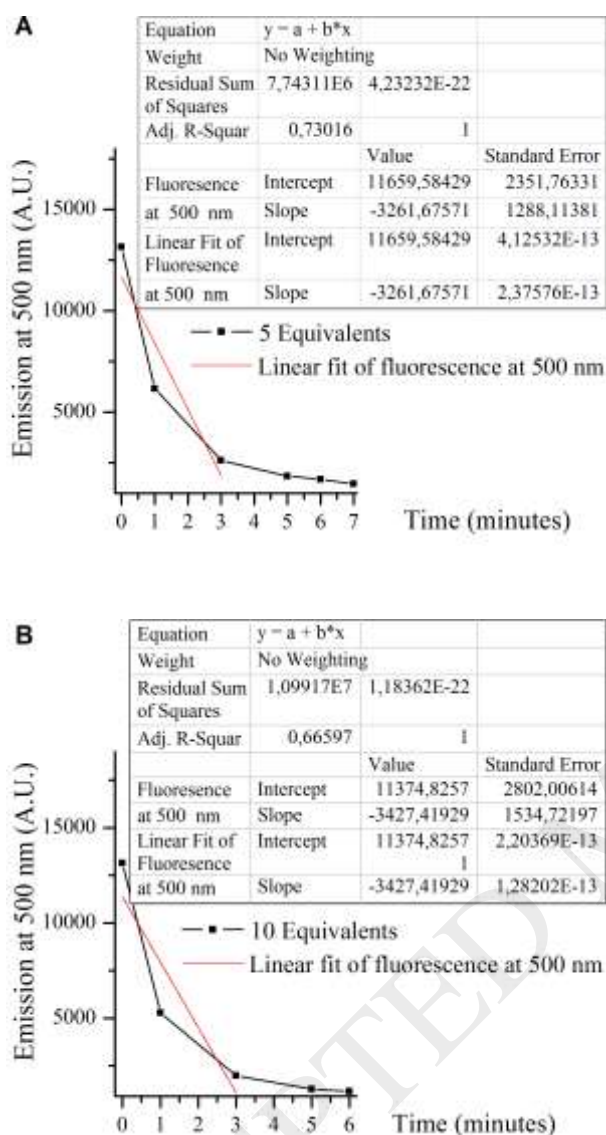




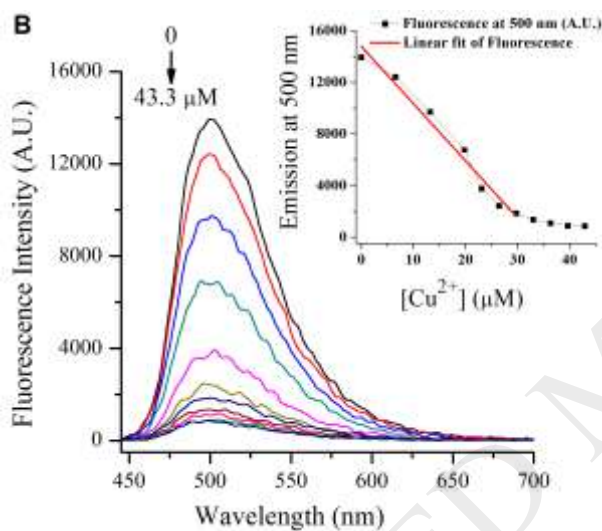
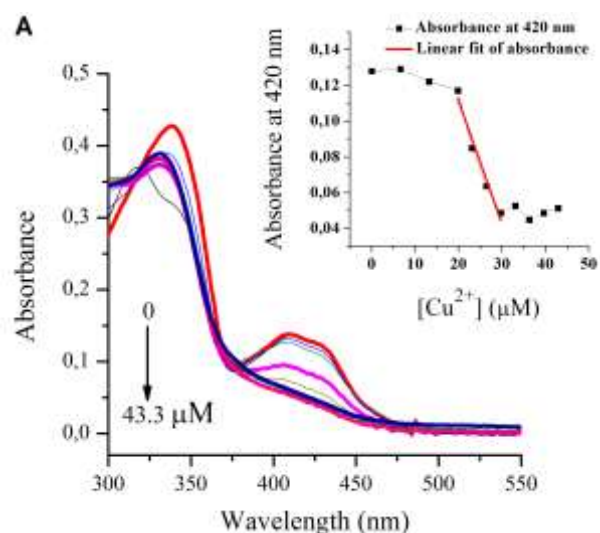
**Fig. 6.** Effect of time on the (A) absorption at 420 nm and (B) fluorescence at 500 nm ( $\lambda_{\text{ex}} = 420$  nm) response of Probe-1 ( $C = 3 \times 10^{-5}$  mol L<sup>-1</sup>) in aqueous solution and borate buffer (0.2 mol L<sup>-1</sup>, pH = 10) towards one equivalent of Cu<sup>2+</sup> ( $C = 3 \times 10^{-5}$  mol L<sup>-1</sup>).



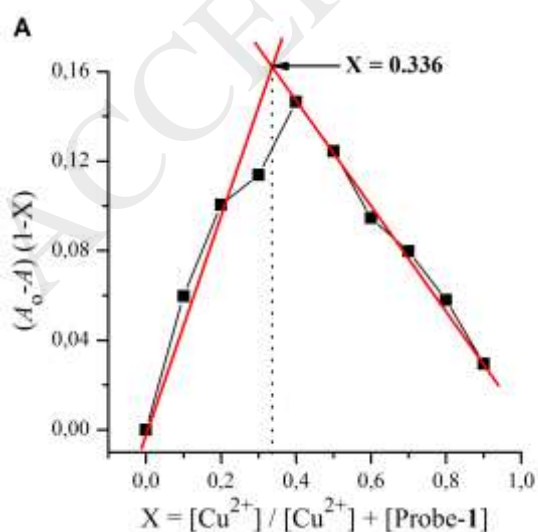
**Fig. 7.** Effect of time on the fluorescence response of Probe-1 ( $\lambda_{\text{ex}} = 420 \text{ nm}$ ) in aqueous solution ( $C = 3 \times 10^{-5} \text{ mol L}^{-1}$ ) and borate buffer ( $0.2 \text{ mol L}^{-1}$ ,  $\text{pH} = 10$ ) towards (A) 5 equivalents ( $C = 1.5 \times 10^{-4} \text{ mol L}^{-1}$ ) and (B) 10 equivalents ( $C = 1.5 \times 10^{-4} \text{ mol L}^{-1}$ ) of  $\text{Cu}^{2+}$ .

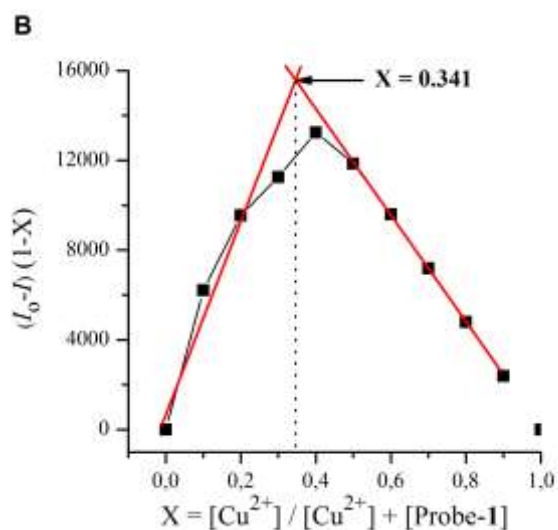


**Fig. 8.** Effect of  $[\text{Cu}^{2+}]$  on (A) absorption and (B) fluorescence ( $\lambda_{\text{ex}} = 420 \text{ nm}$ ) spectra of Probe-1 ( $C = 3 \times 10^{-5} \text{ mol L}^{-1}$ ) in aqueous solution and borate buffer ( $0.2 \text{ mol L}^{-1}$ ,  $\text{pH} = 10$ ). Insets: Titration plots of absorption at 420 nm (A) and emission at 500 nm (B) as a function of  $[\text{Cu}^{2+}]$ .

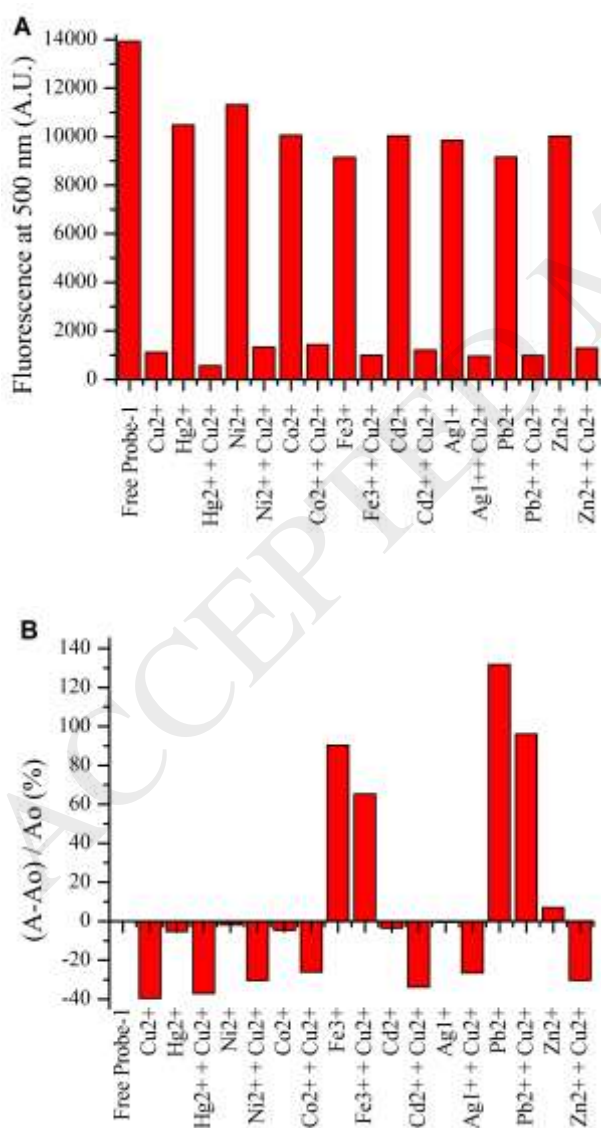


**Fig. 9.** Job's plots by (A) absorbance at 420 nm and (B) fluorescence emission at 500 nm ( $\lambda_{ex} = 420$  nm) at different molar ratio X ( $[Probe-1] = [Cu^{2+}] = 10^{-3}$  mol L $^{-1}$ ) in aqueous solution and borate buffer (0.2 mol L $^{-1}$ , pH = 10).

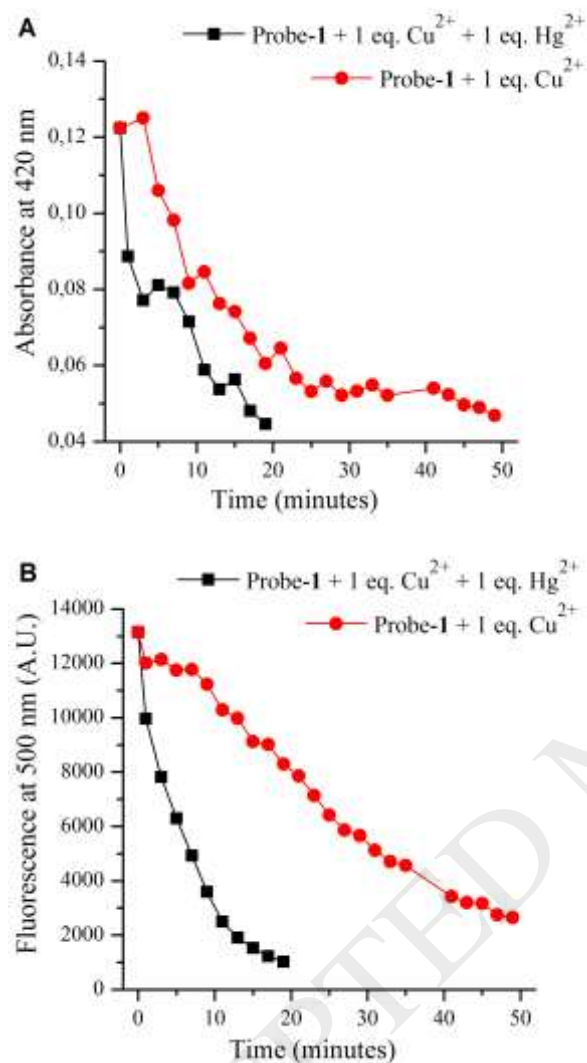




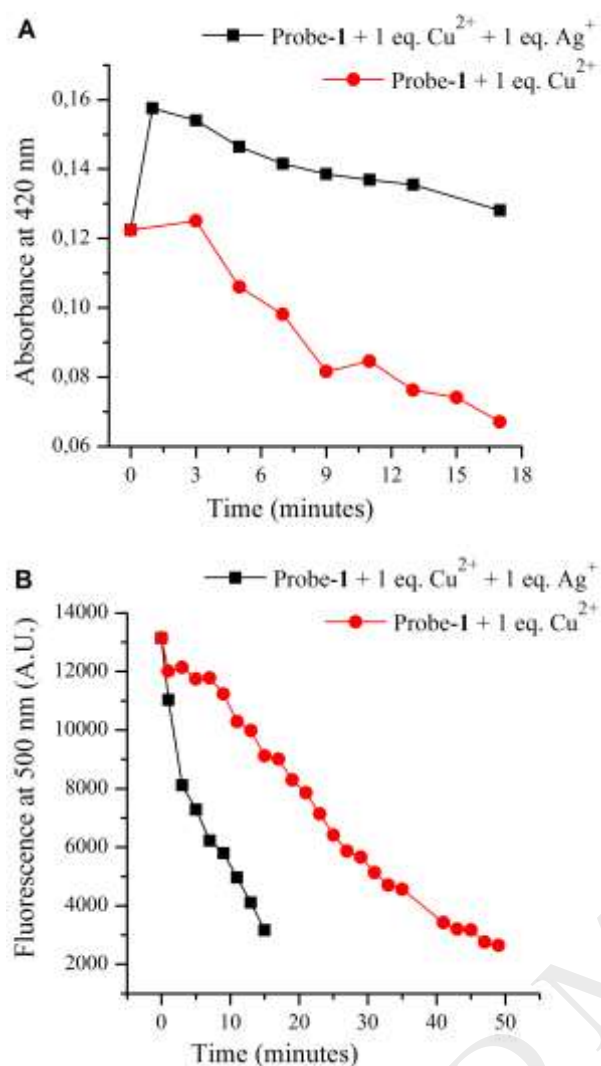
**Fig. 10.** Effect of interfering cations (10 equivalents,  $C = 3 \times 10^{-4}$  mol L<sup>-1</sup>) on (A) emission at 500 nm ( $\lambda_{ex} = 420$  nm) and (B) absorbance at 420 nm of Probe-1 ( $C = 3 \times 10^{-5}$  mol L<sup>-1</sup>) in aqueous solution and borate buffer (0.2 mol L<sup>-1</sup>, pH = 10).



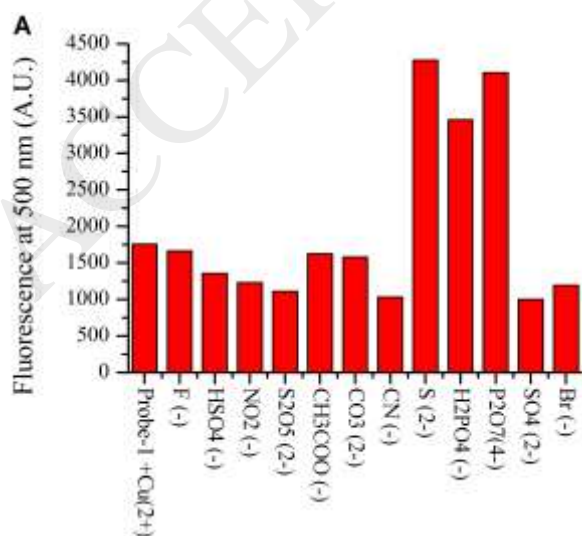
**Fig. 11.** Effect of time in the presence of  $\text{Hg}^{2+}$  (one equivalent,  $C = 3 \times 10^{-5} \text{ mol L}^{-1}$ ) on (A) absorbance at 420 nm and (B) fluorescence at 500 nm ( $\lambda_{\text{ex}} = 420 \text{ nm}$ ) of Probe-1 response in aqueous solution ( $C = 3 \times 10^{-5} \text{ mol L}^{-1}$ ) and borate buffer ( $0.2 \text{ mol L}^{-1}$ ,  $\text{pH} = 10$ ) towards the presence of  $\text{Cu}^{2+}$  (one equivalent,  $C = 3 \times 10^{-5} \text{ mol L}^{-1}$ ).

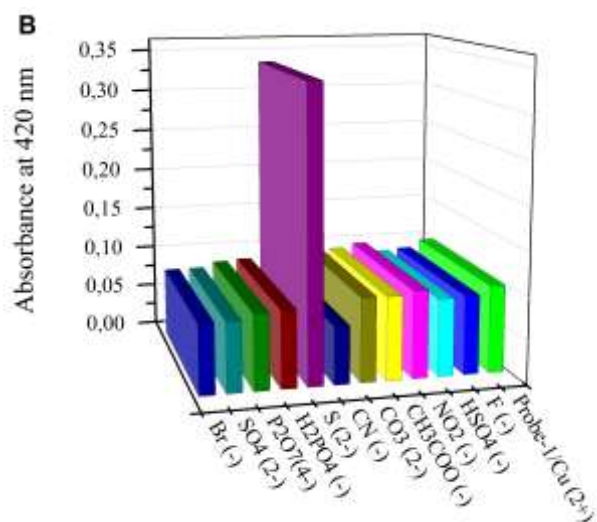


**Fig. 12.** Effect of time in the presence of  $\text{Ag}^{+}$  (one equivalent,  $C = 3 \times 10^{-5} \text{ mol L}^{-1}$ ) on (A) absorbance at 420 nm and (B) fluorescence at 500 nm ( $\lambda_{\text{ex}} = 420 \text{ nm}$ ) of Probe-1 response in aqueous solution ( $C = 3 \times 10^{-5} \text{ mol L}^{-1}$ ) and borate buffer ( $0.2 \text{ mol L}^{-1}$ ,  $\text{pH} = 10$ ) towards the presence of  $\text{Cu}^{2+}$  (one equivalent,  $C = 3 \times 10^{-5} \text{ mol L}^{-1}$ ).

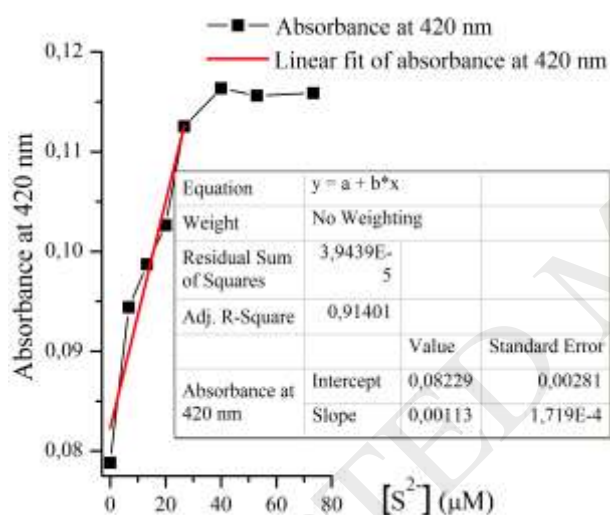


**Fig. 13.** Effect of anions (10 equivalents,  $3 \times 10^{-4}$  M, water) on (A) fluorescence at 500 nm ( $\lambda_{\text{ex}} = 420$  nm) and (B) absorbance at 420 nm of Probe-1 ( $C = 3 \times 10^{-5}$  mol L<sup>-1</sup>) in aqueous solution and borate buffer (0.2 mol L<sup>-1</sup>, pH = 10) in the presence of Cu<sup>2+</sup> (10 equivalents,  $3 \times 10^{-4}$  M, water).

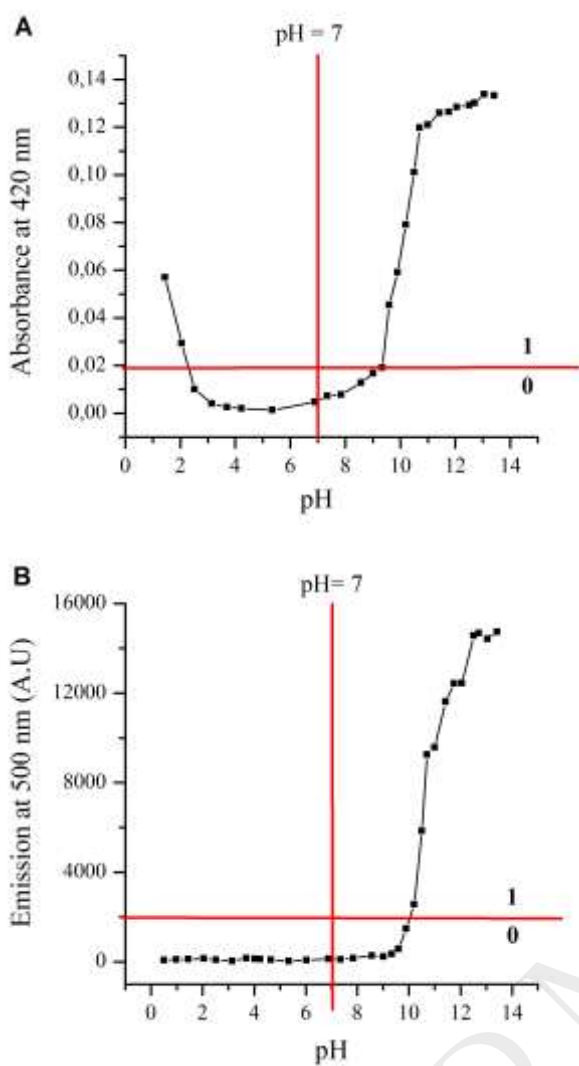




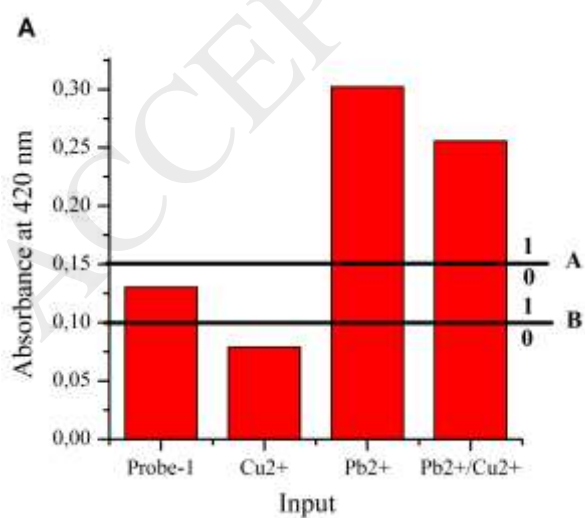
**Fig. 14.** Effect of  $[S^{2-}]$  on the absorbance at 420 nm of the complex of the probe ( $C = 3 \times 10^{-5}$  mol  $L^{-1}$ ) in aqueous solution and borate buffer (0.2 mol  $L^{-1}$ , pH = 10) and  $Cu^{2+}$  ( $C = 1.5 \times 10^{-5}$  M, water).



**Fig. 15.** The changes in (A) absorbance at 420 nm and (B) fluorescence emission at 500 nm ( $\lambda_{ex} = 420$  nm) of Probe-1 ( $C = 1 \times 10^{-5}$  mol  $L^{-1}$ ) in ethanol/water (1:2, v/v) with Acid ( $C = 10^{-1}$  mol  $L^{-1}$ ) and Base ( $C = 10^{-1}$  mol  $L^{-1}$ ) as chemical inputs.



**Fig. 16.** The changes in (A) absorbance at 420 nm and (B) fluorescence emission at 500 nm ( $\lambda_{ex} = 420$  nm) of Probe-1 ( $C = 3 \times 10^{-5}$  mol L $^{-1}$ ) aqueous solution and borate buffer (0.2 mol L $^{-1}$ , pH = 10) with Cu $^{2+}$  and Pb $^{2+}$  ( $C = 3 \times 10^{-4}$  mol L $^{-1}$ ) as chemical inputs.



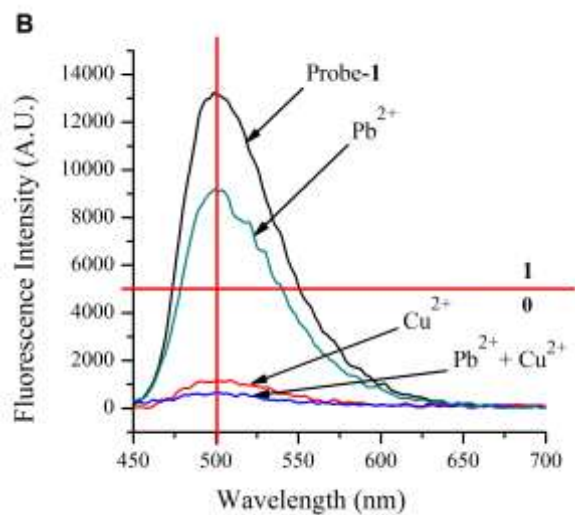
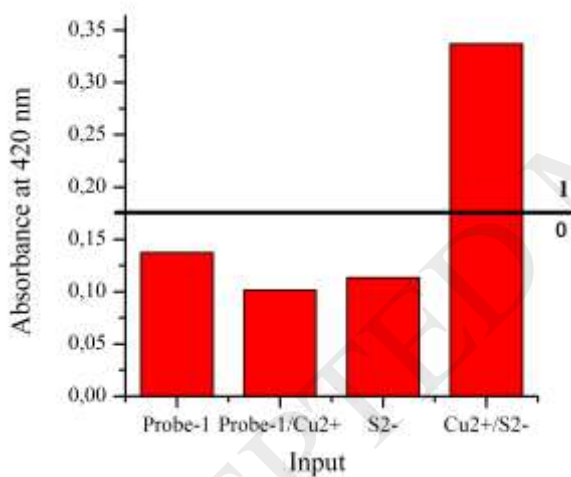


**Fig. 17.** Changes in the absorbance at 420 nm of Probe-1 ( $C = 3 \times 10^{-5} \text{ mol L}^{-1}$ ) in aqueous solution and borate buffer ( $0.2 \text{ mol L}^{-1}$ ,  $\text{pH} = 10$ ) in the presence of  $\text{Cu}^{2+}$  and  $\text{S}^{2-}$  ( $C = 3 \times 10^{-4} \text{ mol L}^{-1}$ ) as inputs.



## Equations

$$\log \left[ \frac{(A_{\max} - A)}{(A - A_{\min})} \right] = pH - pK_a \quad (1)$$

$$\log \left[ \frac{(I_{F \max} - I_F)}{(I_F - I_{F \min})} \right] = pH - pK_a \quad (2)$$

$$QE = (F_0 - F) / F_0 \times 100 \quad (3)$$

$$\frac{1}{I - I_0} = \frac{1}{I_\infty - I} \left[ \frac{1}{K[C]^n} + 1 \right] \quad (4)$$